Toward the Development of Miniaturized Imaging Systems for Detection of Pre-Cancer

Michael R. Descour, Ari H. O. Kärkkäinen, Jeremy D. Rogers, Chen Liang, Ronald S. Weinstein, Juha T. Rantala, Bahattin Kilic, Erdogan Madenci, Rebecca R. Richards-Kortum, Eric V. Anslyn, Russell D. Dupuis, Randy J. Schul, Christi G. Willison, and Chris P. Tigges

Invited Paper

***Abstract*—In this paper, we describe the progress toward the development of miniaturized imaging systems with applications in medical imaging, and specifically, detection of pre-cancer. The focus of the article is a miniature, optical-sectioning, fluorescence microscope. The miniature microscope is constructed from lithographically printed optics and assembled using a bulk micromachined silicon microoptical table. Optical elements have been printed in a negative tone hybrid glass to a maximum depth of 59 μm and an rms surface roughness between 10–45 nm, fulfilling the requirements of the miniature microscope. Test optical elements have been assembled using silicon-spring equipped mounting slots. The design of silicon springs is presented in this paper. Optical elements can be assembled within the tolerances of an *NA* $= 0.4$ miniature microscope objective, confirming the concept of simple, zero-alignment assembly.**

***Index Terms*—Biomedical imaging, biomedical microscopy, hybrid sol-gel meterials, microassembly, microoptics, photolithography.**

I. Introduction

THE AMERICAN Cancer Society estimates that 1 220 100 people will have been diagnosed with cancer in 2000. In the same year, 552 200 persons were expected to succumb to cancer [1]. Despite significant advances in treatment, early detection of cancer and its curable precursors remains the best way to ensure patient survival and quality of life. Thus, highly sensitive and cost-effective screening and diagnostic techniques to identify curable pre-cancerous lesions are urgently needed. Pre-cancers are characterized by morphologic and biochemical changes that include increased nuclear size, increased nuclear-to-cytoplasmic ratio, hyperchromasia, pleomorphism, angiogenesis, and increased metabolic rate. These changes currently can only be assessed through invasive biopsy. Early detection of curable pre-cancers has the potential to significantly lower cancer mortality and morbidity. Many visual exam procedures, such as colonoscopy and bronchoscopy, are routinely used to identify pre-malignant changes and early cancers; however, these techniques do not assess the microscopic and/or biochemical changes which are the hallmark of pre-cancer. Thus, these techniques' sensitivity and specificity are limited.

The long-term goal of our research is to develop a class of miniature microscopes that utilize the interaction of light with tissues in many modalities to image morphology and biochemistry *in vivo*, yielding tools that provide better delineation of tumors. We envision battery-powered, pen-sized multi-modal miniature microscopes (4Ms) designed to specifically image microscopic and molecular features of pre-cancer (see Fig. 1). The proposed miniature microscopes are multi-modal because of their potential for enabling different imaging modalities such as optical sectioning, 3-D spectral fluorescence imaging, and reflectance imaging. The size and cost of these microscopes can be eventually small enough so that they can assist in guiding diagnostic biopsy and in margin detection during tumor resection. 4M devices, suitably adapted, will have broad applicability in many organ sites due to their very compact size and capability for imaging. Because of the easy accessibility of the oral cavity and uterine cervix, we are aiming the initial development of 4M devices to improve detection of pre-cancers in these organ sites. We have shown that both morphologic and biochemical changes that accompany pre-cancer can be probed using reflectance and fluorescence. Therefore, we are designing 4M devices to image both reflected light and autofluorescence.

By way of example, Fig. 1(b) shows a design of a complete 4M device. This 4M device is configured as an optical-sectioning, fluorescence microscope. Excitation light is generated at an integrated light source or alternatively delivered via an optical fiber. The collector mirror captures the available excitation light and images the light source into the aperture stop of the miniature microscope objective, i.e., this is a Koehler-illumination system similar to conventional bench-top microscopes. The collected excitation light passes through a scanning grating, a folding flat mirror, and a dichroic

Manuscript received June 6, 2001 This work was supported by the National Science Foundation (NSF) (BES-0086736) and by NSF SGER ECS-0074578. The work of A. H. O. Kärkkäinen was supported by VTT Electronics, Oulu, Finland.

M. R. Descour, A. H. O. Kärkkäinen, J. D. Rogers, C. Liang, B. Kilic, E. Madenci, and J. T. Rantala are with the Optical Sciences Center, Aerospace and Mechanical Engineering Department, University of Arizona, Tucson, AZ 85721 USA.

R. S. Weinstein is with the Department of Pathology, College of Medicine, University of Arizona, Tuscon, AZ 85721 USA.

R. J. Shul, C. G. Willison, and C. P. Tigges are with Sandia National Laboratories, Albuquerque, NM 87185 USA

R. R. Richards-Kortum, E. V. Anslyn, and R. D. Dupuis are with The University of Texas at Austin, Austin, TX 78712 USA.

Publisher Item Identifier S 0018-9197(02)00616-4.

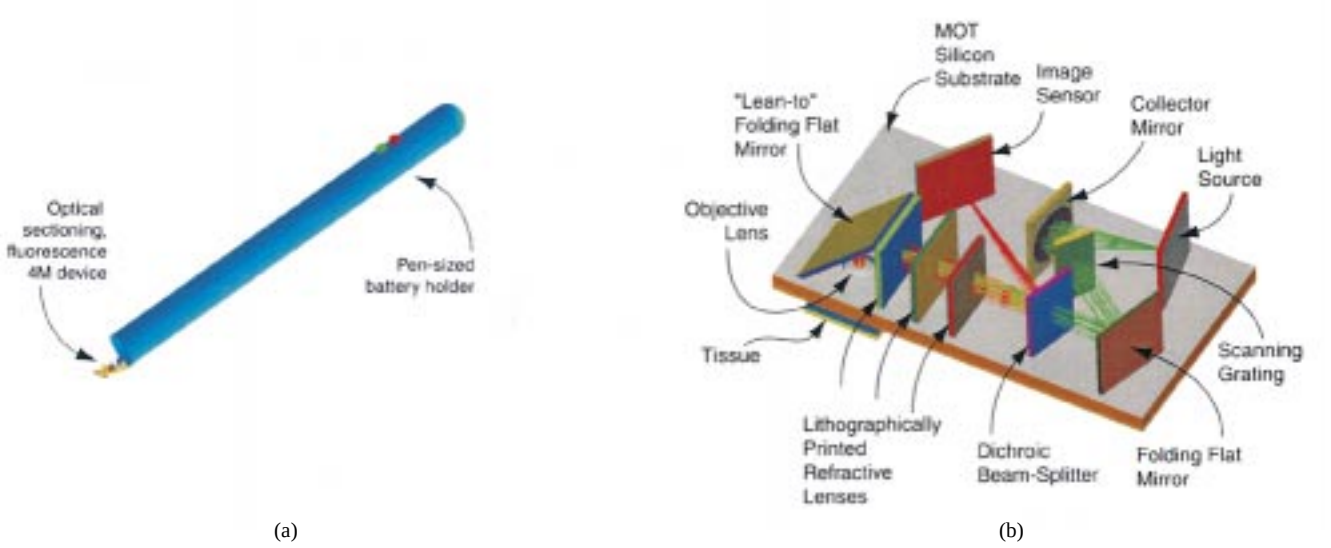

(a) (b)

Fig. 1. Pen-sized miniature microscope. (a) A conceptual, scaled diagram of a pen-sized imaging probe equipped at the tip with a multi-modal miniature microscope (4M). (b) A magnified view of the 4M-device layout. The 4M device measures 9 mm in length, 5 mm in width, and 3 mm in height.

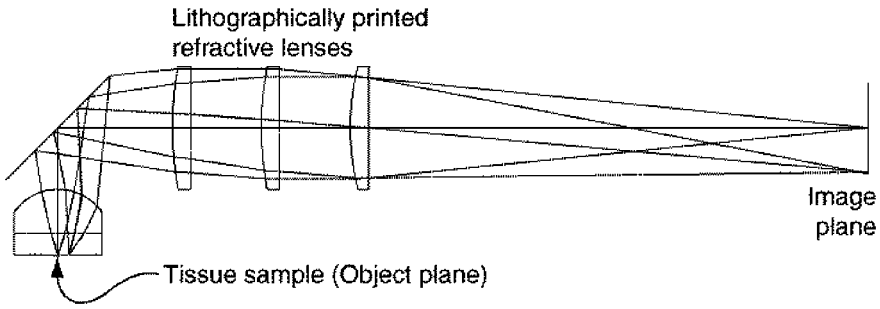

Fig. 2. Optical design of a miniature microscope objective. The figure shows the design form of an $NA = 0.4$, $m = -4$ microscope objective with a field of view of 300 μm. This is the microscope objective used in the complete 4M device shown in Fig. 1.

beam-splitter before being directed by the microscope objective onto the tissue being examined. The microscope objective in Fig. 1(b) consists of three lithographically printed lenses, a folding flat mirror, and a plano-convex objective lens. The scanning grating provides structured illumination of the tissue and therefore the optical-sectioning capability. Fluorescent emission from the tissue propagates back through the microscope objective. The dichroic beam-splitter reflects the emitted longer wavelengths to an image sensor in the form of a photodetector array. All active and passive components of the 4M device are embedded in a microoptical table (MOT) that is micromachined in a 5 mm by 9 mm silicon chip.

This paper describes the technology foundations of 4M devices such as the one shown in Fig. 1(b). Section II contains a discussion of optical-design guidelines associated with miniature imaging systems. A resultant microscope-objective design is shown in Fig. 2. Sections III and IV emphasize simple assembly and fabrication methods of miniature imaging systems. Section III describes progress on the development of an accurate, "snap-together" method of building optical systems (Figs. 3 and 4). Preliminary assembly results are presented (see Figs. 5 and 6) and are compared to the requirements of the optical system shown in Fig. 1(b). Section IV provides a description of lithographic printing of refractive lenses and opto–mechanical structures using hybrid-glass materials (Fig. 7). The most recent results of printing mechanical and optical structures are shown in Figs. 8 and 9, respectively.

II. Optical Design Considerations

Miniaturization of a microscope system requires an instrument-design approach that differs fundamentally from the design of a conventional compound microscope [2].

A compound microscope is a visual instrument that consists of a microscope objective and an eyepiece. The image sensor is assumed to be the human eye. The microscope objective forms an intermediate, real image at the front focal plane of the eyepiece. The eyepiece presents to the eye a virtual image located between a minimum viewing distance of 250 mm (the so-called *near point*) and a maximum viewing distance of infinity.

The visual magnification m_v of a compound microscope is given by $m_v = m_{\rm obj} m_{\rm eye}$, where $m_{\rm obj}$ is the transverse magnification of the microscope objective and $m_{\rm eye}$ is the magnifying power of the eyepiece. By considering the eye's visual acuity (0.3 mrad), the near-point viewing distance (250 mm) and the Rayleigh resolution criterion at $\lambda = 680$ nm, the optimal visual magnification is calculated to be $m_v \approx 180 NA_{\rm obj}$ [2]. Strictly speaking, visual magnification above this optimal threshold does not reveal further information about the object. However, a rule followed for comfortable viewing is $m_v \approx$

$500NA_{\rm obj}$. Note that a given visual magnification m_v can be achieved through different combinations of objectives and eyepieces. Typical eyepiece magnifying power $m_{\rm eye}$ is $10\times$. Higher values of m_{eye} are undesirable because of reduced eye relief and more complex optical designs. Typical dry microscope objectives satisfy the relation $m_{\rm obj} \approx 50NA_{\rm obj}$ [2], [3].

A requirement of miniaturizing a microscope is that the distance between the object plane and the image plane, the so-called *throw*, be minimized. Throw, T, is itself a function of m_{obj}, i.e., $T = -f_{\rm obj}\, m_{\rm obj}((1/m_{\rm obj}) - 1)^2$, where f_{obj} is the effective focal length of the microscope objective. The minimum throw occurs at $m_{\rm obj} = -1$ and $T_{\rm min} = 4f_{\rm obj}$. This is not a practical solution because it requires that spacing between image-plane detector elements be equal to the desired sampling at the object plane, e.g., on the order of micrometers. Consequently, $|m_{\rm obj}|$ needs to be greater than unity but remain low to miniaturize the microscope size. This constraint is not present in the design of conventional compound microscopes, where $|m_{\rm obj}| > m_{\rm eye}$.

In the 4M approach described here, the image recorded on an image sensor will be magnified electronically rather than optically for viewing by eye, i.e., the image will be displayed resampled and expanded. Such electronic magnification is equivalent to the optical function performed by an eyepiece. In each case, the user perceives the final image at a comfortable viewing distance, e.g., 250 mm.

The following quantitative example clarifies these considerations. Given $NA_{\rm obj} = 0.3$, then $m_v = 150$. The transverse magnification of the miniature microscope $m_{\rm obj}$ is defined by the ratio of image size to object size. For the 4M device in Fig. 1(b), $m_{\rm obj} = -4$. This value of $m_{\rm obj}$ means that the recorded image needs to be scaled up for viewing by a factor of $m_{\rm eye} = 37.5$ to yield $m_v = 150$. The field of view of the microscope is given as 250 μm on a side and the size of the image at the image sensor is, therefore, 1000 μm on a side [see Fig. 1(b)]. The final image displayed on a video monitor, assuming a viewing distance of 250 mm, measures 37.5 mm on a side. The resolution of the 4M device is currently expected to be detector-limited rather than diffraction-limited. The spacing between two adjacent detector elements, assumed to be 10 μm, exceeds the resel distance at the image plane [4]. However, we expect that detector spacing (a.k.a., detector pitch) will continue to decrease along with the continuing decrease in the minimum feature size of integrated circuits.

A. Optical Design of Miniature Microscope Objective

Based on the above considerations, we have developed a series of microscope-objective designs that feature a combination of high numerical aperture and low transverse magnification. The high NA yields high spatial resolution. The low transverse magnification keeps the size of the microscope objective small. Typical distances from the tissue sample to the image plane are on the order of 6–8 mm.

A typical miniature microscope-objective design is shown in Fig. 2. The design consists of a commercial plano-convex lens that is followed by a folding mirror and three lithographically printed lenslets. The objective is designed to function with water as an immersion medium.

TABLE I
SELECTED TIGHTEST ASSEMBLY TOLERANCES ASSOCIATED WITH THE $NA = 0.4$ MICROSCOPE OBJECTIVE SHOWN IN FIG. 2

Tolerance Type	Tolerance Value
Optical element pitch rotation	± 0.46°
Optical element yaw rotation	± 0.46°
Optical element translation along slot	± 10 μm

The form of the microscope objective in Fig. 2 was selected to be compatible with lithographic fabrication of optical elements and bulk-micromachining of a silicon substrate as a microoptical table. In order to increase the NA of the objective, the lithographically printed lenslets need to exhibit an increased sag, i.e., the height difference between the center of the lenslet aperture and the edge. For example, the three lithographically printed lenses in the Fig. 2 design require a sag of 60 μm. The need for increased sag motivated the development of new hybrid glasses described in Section IV.

Table I lists representative tightest assembly tolerances associated with the microscope objective shown in Fig. 2. These tolerances have to be met for the optical system in Fig. 2 to remain diffraction-limited in imaging performance.

III. ASSEMBLY OF MINIATURE OPTICAL SYSTEMS

Miniaturization of microscopes requires a simple and accurate method of building such optical systems. We are developing a novel method of constructing compact, 3-D imaging systems that consist of optical elements, e.g., lenses and mirrors, micro-mechanical components, photo-detectors, and light sources [5]. All these components, both active and passive, are mounted on a specially prepared substrate [see Fig. 1(b)]. We refer to the substrate as a MOT, in analogy with the macroscopic version routinely used in optics laboratories. The MOT is a zero-alignment microscopic optical-system concept. In practical terms, the zero-alignment concept translates into assembly errors that are smaller than the tolerances dictated by the performance of the optical system (e.g., see Table I). Very low assembly errors will be achieved through positioning features on each 4M-device component and a silicon spring in each component mounting slot (see Figs. 3 and 4). The accurate positioning of each optical element relative to other optical elements on the MOT is achieved through the sub-micron-precision layout of the photomask from which the MOT is made.

The cross section of each mounting slot includes a silicon spring (Fig. 3). Each mounting slot also features V-shaped guide channels that match complementary positioning features in the optical element that is inserted within the slot (see Figs. 5 and 7). The role of the silicon spring is to press the positioning features on an optical element into the V-shaped guide channels, thereby achieving accurate positioning of the optical element. The depth to which the optical element is inserted into the slot is defined by stops printed on the optical element. We expect to eventually achieve optical-element alignment to an accuracy of ± 2 μm in position and ± 0.5 mrad in rotation using the assembly method illustrated in Figs. 3 and 4.

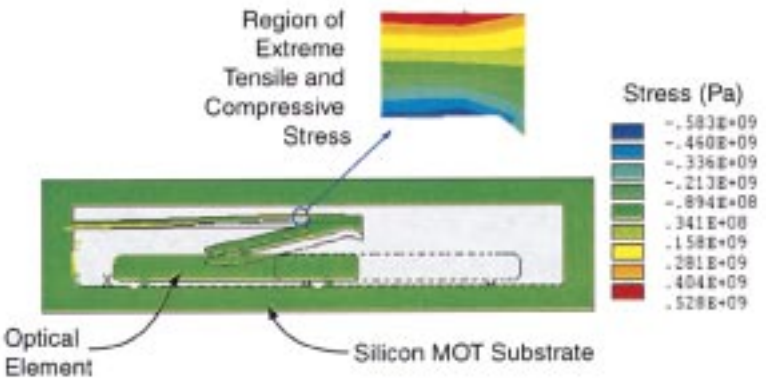

Fig. 3. Silicon-spring displacement and the normal stress in the horizontal direction. The optical element is shown in its penultimate position. The highest tensile stress (shown in red) is predicted to occur at the top of the spring in this diagram. The predicted maximum tensile stress in the silicon spring is less than the failure stress of silicon, thus validating the design of the silicon spring. The thickness of the optical element is 150 μm.

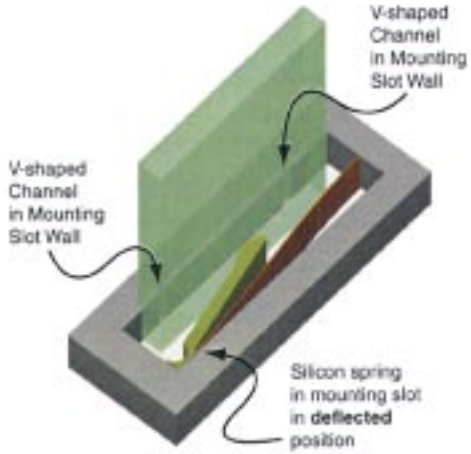

Fig. 4. Assembly of optical elements and MOT substrate.

Fig. 3 serves to illustrate the current assembly method from a top-view perspective. An optical element is first inserted into the open section of the mounting slot. The initial positions of the optical element and the silicon spring are indicated by clear outlines of these two structures. Next, the element is translated under the silicon spring. The penultimate positions of the optical element and the silicon spring are shown by filled-in, green outlines of the optical element and the silicon spring. At this stage, the stresses in the silicon spring reach a maximum value. In the final step, the positioning features on the optical element are press-fitted into the V-shaped grooves that are part of the mounting-slot cross section.

A collection of silicon-spring mounting slots were fabricated. The silicon-spring designs are most readily distinguished by the minimum thickness of the beam segment of the spring. The minimum thickness occurs within the circled region in Fig. 3. We experimented with minimum-thickness values ranging from 30 to 80 μm. In each case, the deflection of the spring was adjusted to not exceed the failure stress of silicon. The forces exerted by the silicon spring on the optical element within the mounting slot ranged from 0.0175 N (30-μm minimum-thickness spring) to 0.116 N (80-μm minimum-thickness spring).

Fig. 5 shows two experimental results of the procedure for assembly of optical elements into the MOT. In this case, test elements coated with a hybrid glass were printed with positioning features using a *binary* photomask. As a result, the positioning features have a rectangular cross-section that measures 35 μm

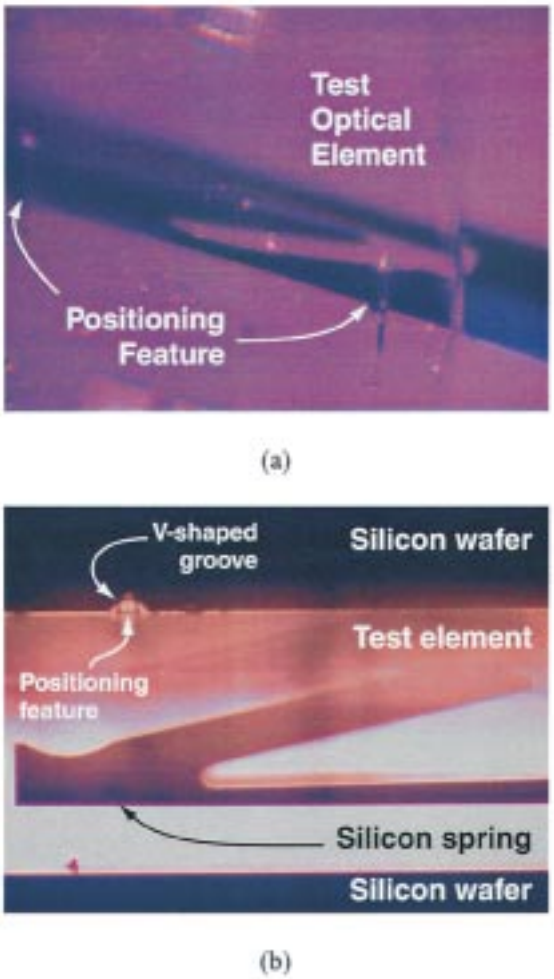

Fig. 5. Implementation of positioning features. (a) Perspective view of a partially inserted, 150-μm-thick glass plate patterned with two rectangular-cross-section positioning features. (b) Top view of the same glass plate, now fully inserted into the mounting slot. Note the fit of the 50-μm-wide positioning feature into a V-shaped groove designed in the cross section of the mounting slot. The width of the narrowest section of the silicon spring is 40 μm.

TABLE II
MEASURED POSITIONING ACCURACIES OF THE ASSEMBLED TEST ELEMENTS IN FIG. 5

Position	Test-element Position Measurement
Pitch rotation	0.44° ± 0.02°
Yaw rotation (Left)	−5 arc min ± 2 arc min
Yaw rotation (Right)	5 arc min ± 2 arc min
Translation along slot	3 μm ± 1 μm

in thickness and 50 μm in width [see Fig. 5(b)]. The rectangular positioning features fit into a V-shaped groove that is etched as part of the mounting slot. The resultant positioning accuracy of a test element is reported in Table II.

The pitch rotation equals the tolerance calculated for the microscope objective shown in Fig. 2. The measured angle is partially the result of a broadening of the mounting slot with depth within the silicon wafer. We predict that the pitch angle can be reduced by adjusting the height of the positioning features to compensate for the observed broadening.

The yaw rotations were measured in the proximity of the left V-shaped groove and the right V-shaped groove (see Figs. 3 and 4) in the mounting slot. High-magnification images of the positioning feature within a V-shaped groove were used to estimate the magnitudes and signs of the yaw rotations [see Fig. 5(b)]. A negative value of the yaw-rotation angle indicates clockwise rotation. The angles are referenced to the edge of the mounting slot etched in the silicon substrate. The measurements indicate that the yaw rotation of the inserted element is small compared to the acceptable tolerance (see Table I). Furthermore, the change in the sign of the yaw-rotation angle indicates a deflection of the optical element caused by the force applied by the spring. The deflection is estimated to be between 1–2 μm at the midpoint between the two positioning features located 1500 μm apart.

The translation along the slot was also measured using high-magnification images of the positioning feature within a V-shaped groove. The position accuracy can be further improved by using the intended circular cross-section positioning features rather than positioning features with a rectangular cross-section as shown in Fig. 5(b).

The position measurements compare favorably with the assembly tolerances listed in Table I. Further characterization of assembly accuracy is required. Nevertheless, the data collected thus far support the hypothesis that simple, zero-alignment assembly of miniature imaging devices is possible.

Fig. 6 shows progress on the fabrication and assembly of a complete microscope objective according to the design of Fig. 2. Fig. 6(a) shows the layout of the microscope objective isolated from other microscope components as presented Fig. 1(b). Fig. 6(b) shows a segment of a silicon wafer etched with an aperture and three slots that will accommodate the optical elements needed to build the objective in Fig. 6(a). The mounting slots are separated by 800 μm. The diameter of the objective-lens aperture is 1000 μm. Fig. 6(c) shows a mock-up of the final microscope-objective. At this stage, a commercial plano-convex glass lens has been cemented into the round aperture. Furthermore, a 150-μm-thick glass plate has been inserted into each of the three mounting slots. In the final configuration, each glass plate will have a height of 2 mm above the surface of the MOT silicon wafer and a width of 2 mm.

IV. FABRICATION OF MICRO-OPTICS

Our preferred approach to fabrication of microoptical and opto–mechanical structures is based on simultaneous printing of such structures using lithography and the hybrid sol–gel method (Fig. 7) [6], [7]. Conventionally, the fabrication of microoptical glass structures is carried out by a multi-step process that includes exposure of a deposited resist film through a photomask, development, and wet or dry etching transfer of the optical structure into the substrate material [8]–[10]. The hybrid sol–gel method has the unique potential for simultaneous fabrication of microoptical and opto–mechanical structures by UV patterning in a single lithography step [11]: No etching transfer of patterned structures is required when using the hybrid sol–gel method. The elimination of the etching–transfer step potentially improves the surface quality of the finished microoptical elements and speeds up the fabrication process even when very thick structures are fabricated.

We have recently demonstrated the fabrication of micro-lens arrays with lens thicknesses up to 100 μm, using photosensitive, negative-tone hybrid glass materials and grayscale lithography [12], [18]. Previously, we have also patterned diffractive optical elements using binary photomasks [see Fig. 7(a)]. Recent binary-photomask patterning experiments demonstrate structure thicknesses greater than 100 μm and a rms surface roughness in the range of 10–20 nm [see Fig. 8]. High film thicknesses are a prerequisite to optical elements of greater optical power, i.e., shorter focal length. Reduced rms surface roughness means a reduction in undesired scattering from lithographically fabricated optical elements. These results in patterning of hybrid glass with a grayscale photomask indicate that we have reached a patterned thickness of significant practical value. The optical design shown in Fig. 2 requires a maximum patterned peak-to-valley thickness, i.e., maximum sag, of 60 μm. The positioning features require a maximum patterned depth of approximately 35 μm.

A. Patterning With Binary Photomasks

When using a binary photomask and a mercury UV lamp in the exposure step, fabrication of binary optical structures can be performed. Fig. 7 shows an early version diffractive-lens element and a recent test element, both patterned using a binary photomask and mercury UV-lamp exposure. Both elements contain positioning features that are used in the assembly procedure outlined in Section III. Fig. 7(a) shows an earlier design in which the positioning features were recessed relative to the surface of the optical element. Fig. 7(b) shows the current design in which all hybrid-glass material is cleared from the substrate, leaving behind protruding positioning features (see Fig. 5). The optical surface and the positioning features are printed simultaneously using the same photomask, thus ensuring sub-micron alignment of the two.

(a) (b) (c)

Fig. 6. The first step: a miniature microscope objective. (a) Scaled layout of a miniature $NA = 0.4$, $m = -4$ microscope objective. (b) Silicon MOT substrate micromachined with an objective-lens aperture and three mounting slots. (c) Partially assembled miniature microscope objective.

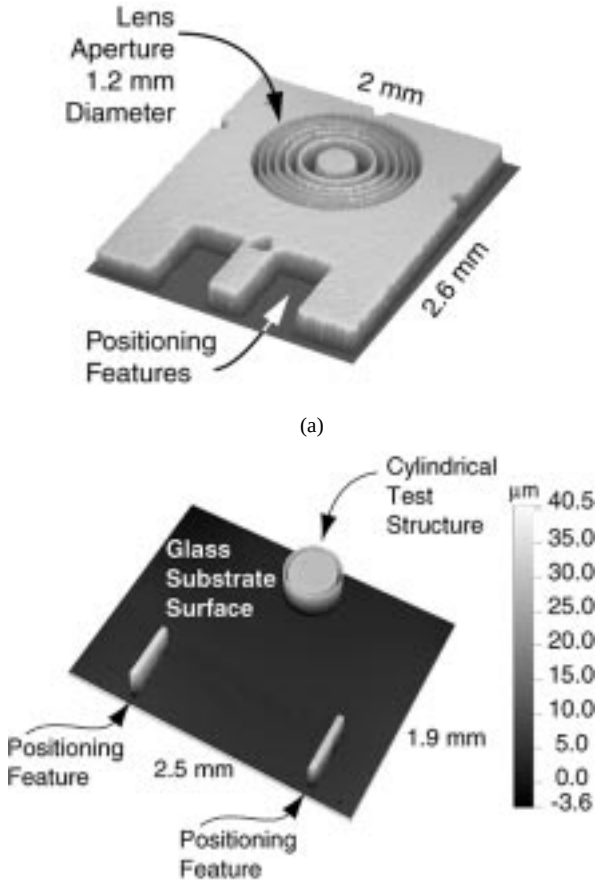

(a) (b)

Fig. 7. Lithographically patterned optical elements. (a) A microoptical element patterned in hybrid glass material on a 150-μm-thick glass substrate. The thickness of the hybrid material is 17.8 μm. The positioning features are of an earlier, recessed design [11]. (b) A more recent test element made with hybrid glass material patterned to a depth of 34 μm. The positioning features now protrude from the substrate.

Fig. 8 shows current results obtained with binary-photomask patterning of hybrid glass. Thicknesses greater than 100 microns have been achieved. Fig. 8(a) shows a 1000-micron diameter cylindrical test feature patterned to an average height of 110 microns. Fig. 8(b) shows positioning features patterned to an average height of 118 μm. Fig. 8(c) shows height data along the profile shown in Fig. 8(b).

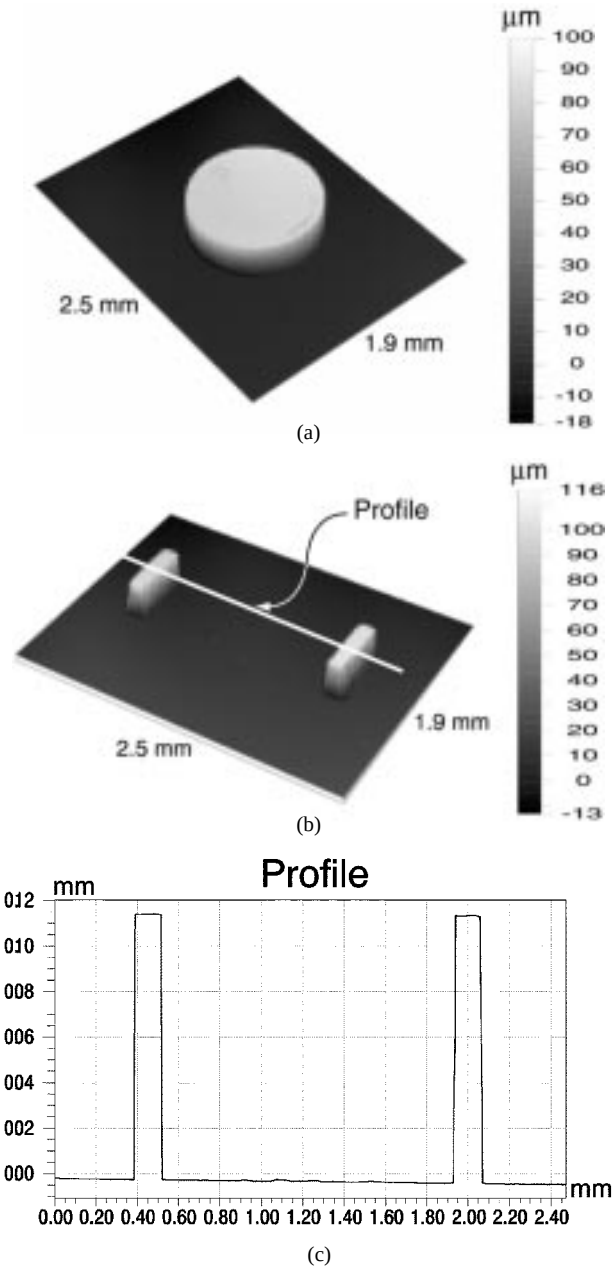

(a) (b) (c)

Fig. 8. Lithographically patterned opto–mechanical structures using binary photomasks.

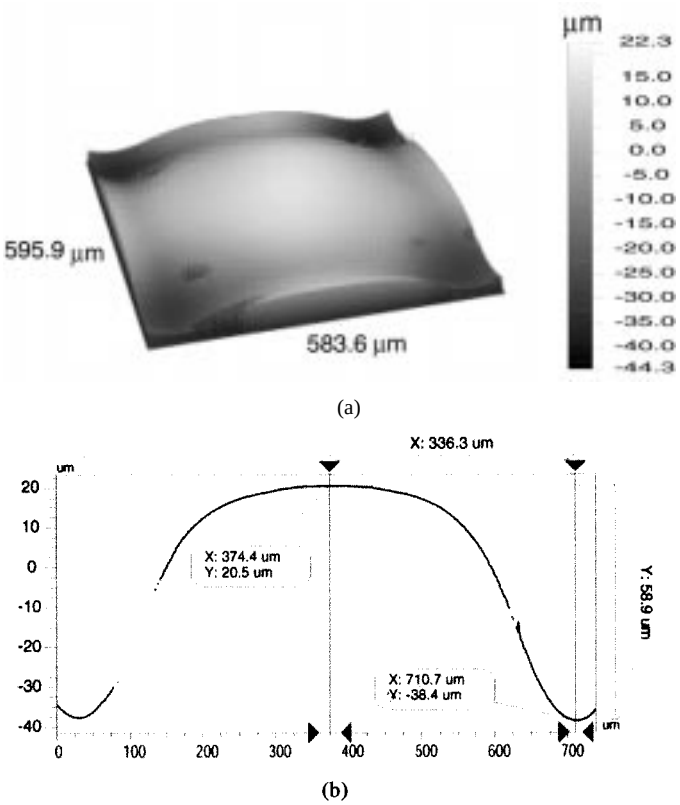

Fig. 9. Segment of a lenslet array patterned in hybrid glass using a grayscale photomask. Each lenslet aperture is a square measuring 240 μm on a side. (a) Isometric view of the grayscale-patterned surface. (b) Diagonal profile of the surface. Missing data occur due to regions of high slope on the patterned surface.

B. Fabrication of Lenslets Using Grayscale Photomasks

The fabrication of optical structures with varying thickness, e.g., lenslets, cannot be performed by using just a single binary photomask. A grayscale photomask has to be used in such 3-D-structure fabrication. The features in a grayscale photomask contain zones that have different transmission values or equivalently, different optical densities. In our case, when fabricating convex lenses using negative tone hybrid glass material, the grayscale photomask exhibits the highest transmission value in the center of a lens pattern and the lowest transmission value at the edge of the lens aperture. Mask transmission decreases gradually between the center and the edge of the lens.

This spatial distribution of mask transmission and, therefore, exposure dose leads to full polymerization of the hybrid glass material in the center of the lens pattern and a gradually decreasing extent of material polymerization toward the edges of the lens pattern. A decrease in the extent of polymerization decreases the thickness of the developed structure and a convex lens shape is fabricated.

Fig. 9(a) shows a surface-topography measurement of a lenslet patterned using a grayscale photomask and mercury UV-lamp exposure. Fig. 9(b) shows a profile of the same lenslet. The achieved patterned depth in this case was 59 μm. The rms surface roughness was measured to be in the range of 10–45 nm.

Grayscale lithography permits the fabrication of nearly arbitrary optical surfaces, e.g., aspheric surfaces and non-rotationally symmetric surfaces. The surface shown in Fig. 9(a), for example, is highly aspheric. A wide selection of surface types offers additional freedom in the design of optical systems that are no longer constrained to consist entirely of spherical surfaces. A desired surface figure can be printed by appropriately choosing the optical densities of circular zones on the grayscale photomask.

We evaluated the surface figure in Fig. 9(a) by estimating the departure of that surface from rotational symmetry. We fitted the surface shown in Fig. 9(a) with a Zernike-polynomial expansion [13]. Specifically, a surface model consisting only of four rotationally symmetric Zernike polynomials was subtracted from the measured surface topography after removal of tilt. The four rotationally symmetric Zernike polynomials were $Z_1(\rho) = 1$, $Z_4(\rho) = \sqrt{3}(2\rho^2 - 1)$, $Z_{11}(\rho) = \sqrt{5}(6\rho^4 - 6\rho^2 + 1)$, and $Z_{22}(\rho) = \sqrt{7}(20\rho^6 - 30\rho^4 + 12\rho^2 - 1)$, where ρ is a radial coordinate normalized by the aperture radius. We found that the greatest departures from rotational symmetry surface occurred near the interfaces between adjacent lenslets in the array. For example, within a subaperture of 175-μm radius, the peak departure from a rotationally symmetric surface was 1.6 μm. The corresponding rms departure from rotational symmetry was 300 nm. We anticipate a reduction in the departure from rotational symmetry when isolated lenslets such as those required by the optical design of Fig. 2 are printed.

C. Hybrid Glass Material

The negative tone hybrid glass materials are used to fabricate optics and opto–mechanics structures. These hybrid materials contain an inorganic base matrix that is prepared by hydrolysis and condensation of alkoxysilanes. The inorganic base matrix is provided with side chains containing terminal carbon double bonds that provide the material with photopolymerizability. In addition, acrylate monomers can be added to the material to increase the crosslinking density of the prepolymer solution. The viscosity of the prepolymer solution needs to be high to result in structures of large thickness. In addition, the material adhesion to the substrate material, e.g., glass, has to be high. The adhesion problems of the hybrid glass material are associated with the densification, e.g., shrinking, of the patterned hybrid glass structures during the final baking step.

By careful design and control of the hybrid glass material's synthesis, we have demonstrated the fabrication of opto–mechanical and optical structures with large thicknesses (see Figs. 8 and 9). A more detailed description of the material synthesis is given elsewhere [12].

The hybrid glass material features an index of refraction of 1.53 at 632.8 nm. The fabricated surfaces exhibit a rms surface roughness in the range of 10–45 nm. The transmission of a 150-μm-thick film of this hybrid glass material deposited on a 1.1-mm-thick glass substrate is greater than 97% at wavelengths ranging from 450 to 1600 nm. An uncoated glass substrate was used as a reference in the transmission measurements.

V. Summary

We have presented progress toward the construction of simple, potentially low cost, miniature imaging devices that are

based on novel materials and microfabrication technologies. We have reported a "snap-together," zero-alignment method of assembling optical elements using a bulk micromachined silicon substrate in the role of a microoptical table. The assembly of compound optical systems such as a miniature microscope objective is assisted by the use of silicon springs that promote accurate positioning of individual optical elements (Fig. 5). The measured position parameters of test elements are equal to or better than the tolerances calculated for the microscope objective shown in Figs. 1(b) and 2.

Optical elements are fabricated using a hybrid glass in a process that eliminates the step of etching transfer from the conventional method of lithographic fabrication of optics. We have reported patterning of the hybrid glass to heights in excess of 100 μm. A height of this magnitude implies that 1-mm diameter refractive optical elements of effective focal length as short as 2.5 mm can be printed using a grayscale photomask. Furthermore, the hybrid glass is well-suited to the fabrication of microopto–mechanical structures that aid in the accurate alignment of multiple optical elements [see Figs. 5(b) and 7(b)].

The inclusion of micro-actuator devices in the context of the microscope-on-a-chip can significantly enhance the capabilities of such a miniature imaging device. The scanning grating shown in Fig. 1(b), for instance, enables optical sectioning by means of structured illumination [14]. Lateral resolution may be enhanced in a similar fashion by means of a grating capable of both translation and rotation [15], [16].

A significant remaining challenge is to combine in one miniature imaging device the capabilities to image a large field of view with low resolution and a smaller field of view with high resolution. In a conventional bench-top microscope, such a combination is effected through a rotating turret equipped with a variety of microscope objectives. The concept of a rotating turret has not yet been translated into the micro-scale but other adaptations exist such as a translating optical subsystem that operates in series with one of two fixed sets of optics [17].

ACKNOWLEDGMENT

The authors gratefully acknowledge the support of Veeco Metrology (www.wyko.com), Tucson, AZ, and Wavefront Sciences, Inc. (www.wavefrontsciences.com), Albuquerque, NM. Sandia is a multiprogram laboratory operated by Sandia Corporation, a Lockheed Martin Company, for the United States Department of Energy under Contract DE-AC04-94AL85000.

REFERENCES

[1] American Cancer Society. (2001). [Online]. Available: http://www.cancer.org/statistics.

[2] D. S. Goodman, "Basic optical instruments," in *Geometrical and Instrumental Optics*, D. Malacara, Ed. New York: Academic, 1988, ch. 4.

[3] M. R. Descour, "Survey of microscope-objective patents from 1976 to 1990," unpublished.

[4] H. Webb and C. K. Dorey, "The pixilated image," in *Handbook of Biological Confocal Microscopy*, J. B. Pawley, Ed., 1995, ch. 4.

[5] R. Levy, M. R. Descour, R. J. Shul, C. L. Willison, M. E. Warren, T. Kololuoma, and J. T. Rantala, "A concept for zero-alignment micro optical systems," in *Proc. Micromachine Technology for Diffractive and Holographic Optics*, S. H. Lee and J. A. Cox, Eds., Sept. 1999, vol. 3879.

[6] J. T. Rantala, P. Äyräs, R. Levy, S. Honkanen, M. R. Descour, and N. Peyghambarian, "Binary phase zone-plate arrays based on hybrid sol–gel glass," *Opt. Lett.*, vol. 23, pp. 1939–1941, 1998.

[7] P. Äyräs, J. T. Rantala, R. Levy, M. R. Descour, S. Honkanen, and N. Peyghambarian, "Multilevel structures in sol–gel thin films with a single UV-exposure using a gray-scale mask," *Thin Solid Films*, vol. 352, pp. 9–12, 1999.

[8] H. Nishihara, M. Haruna, and T. Suhara, *Optical Integrated Circuits*. New York: McGraw-Hill, 1989.

[9] M. Eisner and J. Schwider, "Transferring resist lenses into silicon by RIE," *Opt. Eng.*, vol. 10, pp. 2979–2982, 1996.

[10] E. J. Gratix, "Evolution of a microlens surface under etching conditions," *Miniature and Micro-optics and Micromechanics*, pp. 266–274, 1993.

[11] J. T. Rantala, R. Levy, L. Kivimäki, and M. R. Descour, "Direct UV patterning of thick hybrid glass films for micro-opto–mechanical structures," *Electron. Lett.*, vol. 16, no. 6, pp. 530–531, Mar. 16, 2000.

[12] A. H. O. Kärkkäinen, J. T. Rantala, and M. R. Descour, "Fabrication of micro-optical structures by applying negative-tone hybrid sol–gel materials and grayscale lithography," *Electron. Lett.*, June 2001, to be published.

[13] R. Noll, "Zernike polynomials and atmospheric turbulence," *J. Opt. Soc. Amer.*, vol. 66, no. 3, pp. 207–211, Mar. 1976.

[14] M. A. A. Neil, R. Juškaitis, and T. Wilson, "Method of obtaining optical sectioning by using structured light in a conventional microscope," *Opt. Lett.*, vol. 22, no. 24, p. 1905, Dec. 15, 1997.

[15] M. G. L. Gustafsson, "Surpassing the lateral resolution limit by a factor of two using structured illumination microscopy," *J. Microscopy*, pt. 2, vol. 198, pp. 82–87, May 2000.

[16] J. T. Frohn, H. F. Knapp, and A. Stemmer, "True optical resolution beyond the Rayleigh limit achieved by standing wave illumination," *PNAS*, vol. 97, no. 13, pp. 7232–7236, June 20, 2000.

[17] M. R. Harris, "Scanning confocal microscope including a single fiber for transmitting light to and receiving light from an object," U.S. Patent 5 120 953, June 9, 1992.

[18] A. H. O. Kärkkäinen, J. T. Rantala, A. Maaninen, G. E. Jabbour, and M. R. Descour, "Siloxane based hybrid glass materials for binary and grayscale mask photoimaging," *Advanced Materials*, Oct. 2001, submitted for publication.

Michael R. Descour received the B.S. degree from the University of Colorado, Boulder, in 1990, and the M.S. and Ph.D. degrees from the Optical Sciences Center, University of Arizona, Tucson, in 1992 and 1994, respectively.

He is currently an Associate Professor at the Optical Sciences Center. He was previously with Ball Aerospace Systems Group, Boulder, CO, and Sandia National Laboratories, Albuquerque, NM, as a post-doctoral Appointee. His research group is developing miniature and micro-optical imaging and nonimaging sensors aimed at applications in the health sciences.

Ari H. O. Kärkkäinen received the M.S. degree in organic chemistry (with an emphasis in synthesis and fabrication of organic light-emitting materials and devices) in 2000 from the University of Oulu, Finland, where he is currently working toward the Ph.D. degree in chemistry.

He joined the VTT Electronics Manufacturing Technology Group, Oulu, in 1998. His research interests are in micro-optics (fabrication methods, material synthesis, and fabrication of micro-optical systems), organic thin-film light sources (material synthesis and development of structures and fabrication methods), and sol-gel chemistry. Currently, he is developing novel photoimageable hybrid glass materials for integrated optical systems.

Jeremy D. Rogers received the B.S. degree in physics from Michigan Technological University, Houghton, in 1999. He is currently working toward the Ph.D. degree at the Optical Sciences Center, University of Arizona. His research is in the field of micro-optics and MEMS.

Chen Liang received the B.S degree in optical engineering in 1999 and the M.S. degree in 2000 in optical sciences from the University of Arizona, Tucson, where he is currently working toward the Ph.D. degree in the Optical Sciences Center. His current research includes design and fabrication of miniature optical instruments for biomedical applications.

Ronald S. Weinstein completed his internship and residency at Massachusetts General Hospital, Boston, MA, and was a Teaching Fellow at Harvard Medical School, Cambridge, MA.

From 1970 to 1972, he served as a Major in the U.S. Air Force and was Vice Chairman of Pathology for the Aerospace Medical Research Laboratories in Ohio. He was Chairman of the Department of Pathology at Rush-Presbyterian-St. Luke's Medical Center, Chicago, IL, for 15 years. In July 1990, he became Head of the Department of Pathology, University of Arizona College of Medicine, Tucson. He also serves as Director of the Arizona Telemedicine Program. He is a pioneer in the field of telepathology, and has carried out initial human performance studies on video microscopy and invented robotic telepathology, for which he holds several patents. He was President of the United States and Canadian Academy of Pathology in 1989 and is currently Vice President of the American Telemedicine Association.

Juha T. Rantala received the M.Sc. and Ph.D. degrees in chemistry from the University of Oulu, Finland.

He is Chief Technology Officer of GuideOptics, Inc. Prior to joining GuideOptics, he was with VTT Electronics, Finland, since 1996. During 1997 and 1998, he was a Visiting Scholar at the Optical Sciences Center of the University of Arizona. Since 1999, he has been a Senior Research Scientist of VTT Electronics and has headed activities in advanced materials development for optical and wireless communication applications. He is also a docent and an adjunct faculty member of the Optical Sciences Center of the University of Arizona. In recent years, his research has mostly focused on the development of advanced materials and components for planar optics as well as for electronics and microsystems. Furthermore, his R&D interests include manufacturing and packaging methods and technologies in the areas of modern micro- and electro-optical devices.

Bahattin Kilic received the B.S. degree in mechanical engineering from Istanbul Technical University, Istanbul, Turkey, in 1999. He is currently working toward the M.S. degree in the Department of Aerospace and Mechanical Engineering, University of Arizona, Tucson. His research interests include design and stress analysis of MEMS devices, thermomechanical stress analysis of electronic packages, and composite material mechanics.

Erdogan Madenci received the B.S. degree in mechanical and industrial engineering and the M.S. degree in applied mechanics from Lehigh University, Bethlehem, PA, in 1980, 1981, and 1982, respectively, and the Ph.D. degree in engineering mechanics, from the University of California, Los Angeles, in 1987.

He was a Research Engineer with Northrop Corporation and a Member of Technical Staff at The Aerospace Corporation. He spent one year at the Fraunhofer Institute, Freiburg, Germany, as a Visiting Scientist. He is currently a Professor and Associate Head in the Department of Aerospace and Mechanical Engineering, University of Arizona, Tucson.

Rebecca R. Richards-Kortum received the B.S. degree in physics and mathematics (with highest distinction) from the University of Nebraska, Lincoln, in 1985, and the M.S. and Ph.D. degrees in medical physics from the Massachusetts Institute of Technology, Cambridge, in 1987 and 1990, respectively.

In 1990, she joined the faculty of the Department of Electrical and Computer Engineering and the Biomedical Engineering Program at the University of Texas at Austin. Her research focuses on the application of optical spectroscopy and imaging for detection of precancer.

Dr. Richards-Kortum was the recipient of the Presidential Faculty Fellow Award from the National Science Foundation for excellence in research and teaching in 1992. In 2000, she was elected to the Academy of Distinguished Teachers at the University of Texas at Austin.

Eric V. Anslyn received the B.S. degree in chemistry from California State University, Northridge, in 1983, where he performed on ligand fluxuations in organometallic clusters, and the Ph.D. degree from California Institute of Technology, Pasadena, in 1987, where he worked on the mechanism of olefin metathesis.

From 1987 to 1989, he was a National Science Foundation Post-doctoral Fellow at Columbia University, New York, working with Dr. Ronald Breslow on RNA hydrolysis mechanisms. In 1989, he started at The University of Texas at Austin, where he is now a Full Professor of chemistry and biochemistry.

Dr. Anslyn has been elected to the Academy of Distinguished Teachers at the University of Texas at Austin.

Russell D. Dupuis received the Ph.D. degree in electrical engineering from the University of Illinois at Urbana–Champaign in 1973.

In 1989, he joined The University of Texas at Austin as a Chaired Professor. He currently holds the Judson S. Swearingen Regents Chair in Engineering and is a Professor in the Department of Electrical and Computer Engineering and the Microelectronics Research Center at The University of Texas at Austin. His technical specialties include semiconductor materials and devices, epitaxial growth by metalorganic chemical vapor deposition (MOCVD), and heterojunction structures in compound semiconductors. He is currently studying the growth of III-V compound semiconductor devices by MOCVD, including materials in the InAlGaN/GaN, InAlGaAsP/GaAs, and InAlGaAsP/InP systems. Previously, he has been with Texas Instruments (1973–1975), Rockwell International (1975 –1979), and AT&T Bell Laboratories (1979 to 1989).

Dr. Dupuis is a Fellow of the Optical Society of America.

Randy J. Schul received the B.A. degree in chemistry in 1981 from Rutgers University, NJ, and the Ph.D. degree in chemistry from Pennsylvania State University in 1987.

He is a Principal Member of Technical Staff at Sandia National Laboratories, Albuquerque, NM, in the Microdevice Technologies Department. Previously, he was with AT&T Bell Laboratories, where he was responsible for plasma process development for the fabrication of GaAs digital integrated circuits. His current research interests include silicon micromachining for MEMS, integrated microsystems, and advanced packaging technologies. He is also active in plasma-etch process development for the wide-bandgap group-III nitrides and the development of high-density, low-damage plasma-etch processes for advanced compound semiconductor devices.

Christi G. Willison received the B.S. degree in mathematics from New Mexico State University, Las Cruces, and the M.S. degree in applied mathematics from the University of New Mexico. Albuquerque.

She is currently a Process Engineer at Sandia National Laboratories, Albuquerque, NM, in the Compound Semiconductor Research Laboratory, Microdevice Technologies Department, where she is primarily responsible for deep reactive ion etching of silicon in support of integrated microsystems.

Chris P. Tigges received the B.S. degree in physics from Montana State University, Bozeman, in 1983, and the Ph.D. degree in applied physics in 1988 from Yale University, New Haven, CT, for research in nonequilibrium phenomena in magnetic rare earth compounds.

Between 1988 and 1990, he held a postdoctoral position at Sandia National Laboratories, Albuquerque, NM. In 1990, he joined the permanent staff, where he has contributed in the areas of high-temperature superconductors, high-speed resonant-tunneling power sources, quantum transport analysis in compound semiconductors, as well as thermal, electronic, and mechanical analysis microelectronic and micromachined devices. His recent developments include the design and fabrication support of micro-channel heatpipes, chemistry laboratory on a chip, and bio-sensors.